JOURNAL OF SYNCHROTRON RADIATION

ISSN 1600-5775

In situ synchrotron X-ray powder diffraction for studying the role of induced structural defects on the thermoluminescence mechanism of nanocrystalline LiF

Mostafa El Ashmawy,[a] Hany Amer[a] and Mahmoud Abdellatief[b]*‡

[a]Nuclear and Radiological Regulatory Authority, 3-Ahmed El-Zomor Street, El-Zohour District, Nasr City, 11762 Cairo, Egypt, and [b]Elettra-Synchrotron, SS 14, km 163.5, AREA Science Park, 34149 Basovizza, Trieste, Italy. *Correspondence e-mail: mahmoud.abdellatief@sesame.org.jo

Received 21 May 2015
Accepted 13 January 2016

Edited by V. Favre-Nicolin, CEA and Université Joseph Fourier, France

‡ Current address: Materials Science Beamline, SESAME – Synchrotron Light for Experimental Science and Applications in the Middle East, Allan, PO Box 7, Al Balq'a 19252, Jordan.

Keywords: synchrotron diffraction; thermoluminescence; dislocation density; kinetics; nanocrystalline microstructure.

The correlation between the thermoluminescence (TL) response of nanocrystalline LiF and its microstructure was studied. To investigate the detailed TL mechanism, the glow curves of nanocrystalline LiF samples produced by high-energy ball-milling were analyzed. The microstructure of the prepared samples was analyzed by synchrotron X-ray powder diffraction (XRPD) at room temperature. Then, the microstructure of a representative pulverized sample was investigated in detail by performing *in situ* XRPD in both isothermal and non-isothermal modes. In the present study, the dislocations produced by ball-milling alter the microstructure of the lattice where the relative concentration of the vacancies, responsible for the TL response, changes with milling time. An enhancement in the TL response was recorded for nanocrystalline LiF at high-temperature traps (after dislocations recovery starts >425 K). It is also found that vacancies are playing a major role in the dislocations recovery mechanism. Moreover, the interactions among vacancies–dislocations and/or dislocations–dislocations weaken the TL response.

1. Introduction

The optical properties of lithium fluoride (LiF) are highly attractive in several applications such as integrated optics and colour centre lasers. LiF is also widely used for radiation dosimetry (McKeever, 1983) based on its prominent thermoluminescence (TL) characteristics. For decades, LiF has been subjected to intensive and detailed investigations aimed at understanding the nature of the complex TL phenomenon of such material and other materials as well. For that reason, many models have been proposed discussing various possible internal mechanisms that explain how TL takes place in different materials (Chen & McKeever, 1997; Kirsh, 1992). A simplified explanation could be introduced on the basis of the one-trap one recombination centre (OTOR) model shown in Fig. 1. In the OTOR model, TL material has two metastable states in the wide forbidden gap between the valence and the conduction bands. These metastable states are introduced either by adding some chemical impurities or by introducing structural defects in the lattice. One of such states exists near the conduction band and acts as a trap for electrons while the other exists near the valence band and acts as a trap for holes. When the TL material is excited by radiation, pairs of electrons/holes are generated and are ultimately captured in their respective traps (Fig. 1, left). When the TL material is heated up to appropriate temperatures, the electrons are thermally released to the conduction band and such electrons have two

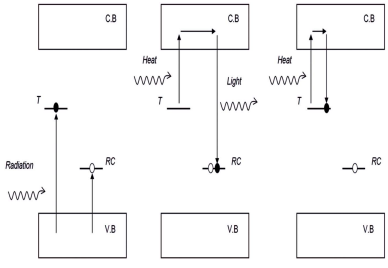

© 2016 International Union of Crystallography

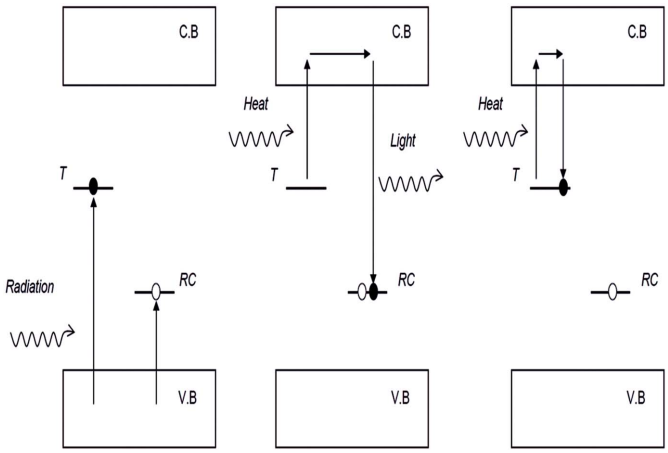

Figure 1
The thermoluminescence process based on the OTOR model. The irradiation produces electron/hole pairs captured in metastable states (left). By heating the material the trapped electron is thermally released to the conduction band and then recombines directly with the hole yielding emitted light (middle), or the electron is retrapped in the same kind of metastable state (right) before recombination.

possible pathways. One way is to recombine directly with the trapped holes yielding emitted light (Fig. 1, middle); for that reason the metastable state that captures the holes is called a recombination centre (RC) and the metastable state that captures electrons is called a trap (T). The other way for the released electrons is to be retrapped by the electron traps (Fig. 1, right) before they are thermally released again to recombine with respective holes at RC; the process in this case could be simply defined as indirect recombination. The energy required to release the electron from its trap to the conduction band is called the activation energy. The relationship between the temperature and the intensity of the released light is known as the 'glow curve' and could be composed of single or multiple superimposed TL glow peaks with each glow peak corresponding to a specific trap, *i.e.* a specific activation energy.

Accordingly, three kinetic models have been proposed according to the OTOR model as follows. First, when the probability of direct recombination dominates the probability of indirect recombination (retrapping before recombination), the case is called a 'first-order' kinetic; a mechanism was proposed by Randall & Wilkins (1945). Second, when the probability of indirect recombination dominates the probability of direct recombination, the case is called a 'second-order' kinetic; such a mechanism was proposed by Garlick & Gibson (1948). Finally, the 'general-order' model, suggested by May & Partridge (1964), when the TL glow curve could be explained neither by the first- nor the second-order kinetic models. Such a model is an empirical one that maintains the characteristics of both first- and second-order kinetic models. Under some condition it is reduced to the 'first-order' model and under other conditions it is reduced to the 'second-order' model. For a detailed mathematical manipulation and analytical formulation of the first-, second- and general-order kinetics, see Kitis *et al.* (1998).

The applicability of any of the kinetic models is highly dependent on the microstructure features, more specifically the defect type and their density; the higher the number of defects in a material the more advanced the kinetic model required to describe the complex glow curve. In such a case, attributing the TL mechanism from such a complex glow curve to a certain type of defect is quite difficult. For that reason, other suitable techniques should be used to obtain more detailed results to correlate the TL mechanism to a certain defect type.

The aim of this work is to obtain a deeper picture of the TL mechanism and its dependency on the microstructure in terms of crystal size and defect density (*e.g.* dislocations). LiF was selected to perform this analysis because of its well known TL properties as well as its quite simple crystal structure. There are many methods of creating structural defects in materials; ball-milling is one such very powerful technique. Plastic deformation (*i.e.* dislocations) is the most common and probable defect type for ball-milling as a result of the energetic impact between powder, vial and balls.

Synchrotron X-ray powder diffraction (XRPD) was selected to follow the change in the crystal size and dislocations density of the ball-milled samples. *In situ* XRPD experiments are appropriate for tracing the crystal growth and dislocations recovery mechanisms under isothermal and non-isothermal conditions. The aim of the *in situ* XRPD is to correlate the TL glow curves with the change of the microstructure details. Moreover, the whole powder pattern modelling approach (Scardi & Leoni, 2002, 2004) was used to perform line profile analysis for the diffraction patterns.

2. Experimental

2.1. Sample preparation

1 g of commercially available LiF powder (99.99% from Sigma Aldrich) was ground in a planetary ball-milling (Fritsch Pulverisette 6) machine operating at high rotational speed (700 rpm). The pristine (as received) LiF powder was ball-milled for several milling times (5, 10, 20, 40, 60 h) in an 80 ml agate container. Twenty balls, each made of agate, with 1 cm diameter, were used. The ball-milled samples were then named as LiF0h for the as-received sample, LiF5h, LiF10h, LiF20h, LiF40h and LiF60h, where the numbers following 'LiF' refer to the overall milling times.

The final product of the milling process is influenced by two main operations. The first is powder fragmentation due to the high impact energy and this operation is responsible for decreasing the crystal size and increasing structural defects. The second operation is the recovery process due to the high milling temperature and such an operation is responsible for the structural recovery by means of increasing crystal size and decreasing structural defects. So, keeping the milling temperature as low as possible is necessary in order to allow the powder fragmentation process to dominate the recovery process during milling. In any case, the two processes tend to balance after a certain milling time where they cancel the

influences of each other, and consequently the crystal size and lattice strain reach certain limits. In order to decrease the milling temperature the milling process was programmed in several time intervals, each of 60 min, and each interval followed by a 30 min pause time. 1 ml ethanol was added to each sample as a milling lubricant to further decrease the milling temperature and to ensure the homogeneity of the ground samples. As discussed elsewhere, this approach of intermittent conventional milling at room temperature proves to give a nanocrystalline powder of LiF (Wall *et al.*, 2014), though the vial, lubricant, milling intervals and breaks are quite different from those used in this study.

2.2. Thermoluminescence

A Thermo Fischer 4500 TLD reader was used to investigate the TL response of both pristine and ball-milled LiF samples. The samples were irradiated by γ-radiation at two doses, 200 Gy and 1000 Gy, using a Co^{60} source at an irradiation rate of 2 KGy h^{-1}. The samples were then compressed into pellets of diameter 5 mm with each pellet weighting 15 mg. At least three pellets of each sample were prepared for measurement to obtain the average of the TL response. Each sample was then heated from room temperature up to about 675 K at 5 K s^{-1} heating rate and the glow curve was recorded. Each sample was measured once more to measure the background, which was subtracted from its glow curve.

2.3. X-ray powder diffraction

Microstructural characterization of the LiF samples was carried out at the MCX beamline (Rebuffi *et al.*, 2014) of the Italian Synchrotron ELETTRA (Trieste). Two different sets of measurements were collected at the same photon energy (12 keV). The first set was collected using Debye–Scherrer geometry. This setup was used to perform fine microstructure line profile analysis at room temperature. A standard sample of NIST SRM 640a silicon in a borosilicate capillary (0.3 mm in diameter) was used to define the instrumental resolution to be considered in the analysis. Then, each sample was prepared in the borosilicate capillary (0.3 mm in diameter). Diffraction data were collected in the range 15–75° 2θ in steps of 0.01°.

A second set of measurements was aimed to investigate the kinetics and crystal growth of a representative pulverized sample (*e.g.* LiF20h) under the influence of heating. In this case, each sample was prepared in a 0.5 mm-diameter quartz capillary. *In situ* XRPD experiments were carried out using the MCX furnace (Riello *et al.*, 2013) while the capillaries containing the samples were placed in the centre of the evacuated furnace. The diffraction signals were received on a curved imaging-plate detector (Fujifilm BAS-IP SR 2025). The furnace experimental parameters (*e.g.* heating rate, exposure time and image-plate displacement after each exposure time) were controlled and programmed. The scanning time for each shot was fixed at 150 s, which was found sufficient to obtain reasonable diffraction intensity statistics.

Two *in situ* experiments were performed. The first one was carried out under non-isothermal conditions using a 10 K min^{-1} heating rate and one shot of diffraction captured every 20 K starting from room temperature up to about 875 K. The other *in situ* XRPD experiment was performed under isothermal conditions at 775 K with the LiF20h sample being firstly heated up at a fast heating rate (30 K min^{-1}); then the sample was kept at the isothermal temperature for about 3 h while one shot of diffraction was captured every 5 min. Upon completion of each experiment, the image plate was developed using a scanner and then the *Fit2D* program was used to convert the images into intensity-pixels powder patterns. The pixels were converted to 2θ using a NIST SRM 640a silicon standard diffraction on an imaging plate using a linear interpolating method between $2\theta_{hkl}$ and their corresponding pixels (Abdellatief, 2013). The refined wavelength obtained from the Si standard pattern measured by the MCX diffractometer was 1.03231 Å. This diffraction of the standard was also used to calibrate the furnace angular resolution and subtracted from the LiF20h structural analysis.

The microstructure was analysed using the whole powder pattern modelling (WPPM) approach (Scardi & Leoni, 2002, 2004) through the *PM2K* program (Leoni *et al.*, 2006). In the modelling, the instrumental profile parameters were fixed and then the line profiles were modelled by considering the crystal size and the lattice strain in terms of dislocations where both aforementioned parameters are the main structural sources of broadening. The crystal size was modelled as spherical crystals of lognormal distribution with two refinable parameters, namely mean μ and variance σ. Equation (1) shows the dislocation average contrast factors A and B for cubic crystals,

$$C_{\rm average} = A + B\,\frac{h^2k^2 + k^2l^2 + h^2l^2}{(h^2 + k^2 + l^2)^2}. \qquad (1)$$

This equation takes into account the anisotropic broadening caused by dislocations as a function of hkl planes. The value of the contrast factor A was calculated analytically ($A_{\rm edge}$ = 0.195, $A_{\rm screw}$ = 0.162, $A_{\rm average}$ = 0.179) as proposed by Ungár *et al.* (1999) and then the parameter B, dislocation density ρ and the average cut-off radius $R_{\rm eff}$ ($R_{\rm eff}$ is the effective cut-off radius of the dislocation) were left as free refinable parameters in the strain model. Beside the crystal size and the lattice strain models, a Chebychev polynomial function with refined coefficients was used to fit the background of the diffraction patterns.

3. Results and discussion

3.1. TL analysis

The samples were exposed to two different doses (200 and 1000 Gy) of γ radiation to examine whether the overall response of the TL behaviour in terms of the integral TL intensity is dose-dependent or not. The overall trend of the TL response in terms of the integral intensity was found to be similar for both doses as shown in Fig. 2, which discloses that the TL response of the pulverized LiF is indeed dose-independent. A significant increase in the integral intensity was detected for short and intermediate milling times (*i.e.* 5 h, 10 h

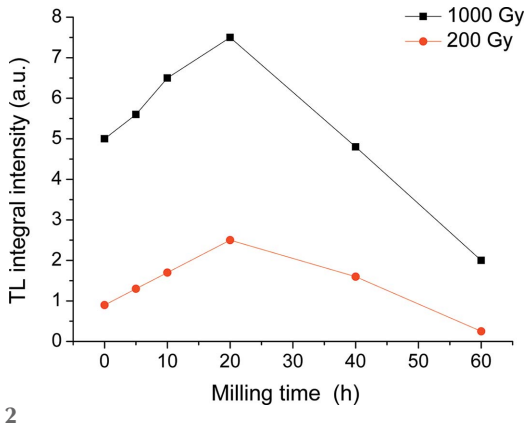

Figure 2
Thermoluminescence integral intensity for the glow curves of all LiF samples as a function of milling time.

and 20 h) and, as the milling time lasts longer than 20 h (*i.e.* 40 h and 60 h), the integral TL intensity shows a significant decrease. Fig. 3 shows a comparison between the resultant glow curves at different doses. As shown in Fig. 3(*a*), there are three prominent peaks around 400, 500 and 610 K in the glow curve of the pristine LiF.

The exact number and positions of the glow peaks (energy traps) cannot be straightforwardly determined. A successful glow curve deconvolution (GCD) could be obtained with the help of the fine features of the glow curve. For example, the asymmetry of the upper part of the first peak (400 K) implies the existence of a small glow peak hidden underneath the first peak. Also, the tilted plateau between the 400 and 500 K peaks suggests the existence of a glow peak between such peaks. Finally, the shoulder just after the 500 K peak and before the 610 K peak implies the existence of another glow peak. Therefore, the glow curve of the pristine samples were analysed assuming the presence of at least six assured convoluted glow peaks.

In fact, tracking the changes in the TL glow curve of a TL material when exposed to different doses is very advantageous in suggesting the most probable kinetic model that interprets how the TL occurs in such material. In other words, when the glow curve does not show a significant change in terms of peak positions and peak shape when the TL sample is exposed to different doses, then the 'first-order' kinetic model is the most probable mechanism (McKeever, 1983; Sunta, 2015). In that case the TL process occurs through direct recombination of trapped electrons with their respective holes trapped at recombination centres (Fig. 1). On the other hand, when there is a significant change in the peaks' positions, the 'first-order' kinetic model is no longer valid to explain the TL process and other kinetic models should be examined to fit the glow curve.

As noticed in Fig. 3(*a*), the maxima and shapes of the glow curves of the pristine LiF samples do not show any significant temperature shift and differ only in the amplitude due to exposure to different doses; this suggests that the TL process of the pristine LiF could be described by the 'first-order' kinetic model. Accordingly, GCD was performed on the glow curve of the pristine samples using the 'first-order' kinetic analytical function given by equation (2) (Kitis *et al.*, 1998),

$$I(t) = I_{\rm m} \exp\left[1 + \frac{E}{KT}\frac{T - T_{\rm m}}{T_{\rm m}} - \frac{T^2}{T_{\rm m}^2} \times \exp\left(\frac{E}{KT}\frac{T - T_{\rm m}}{T_{\rm m}}\right)(1 - \Delta) - \Delta_{\rm m}\right]. \quad (2)$$

In equation (2), $I(t)$ is the intensity at temperature T in K, $I_{\rm m}$ is the maximum peak intensity at maximum temperature $T_{\rm m}$

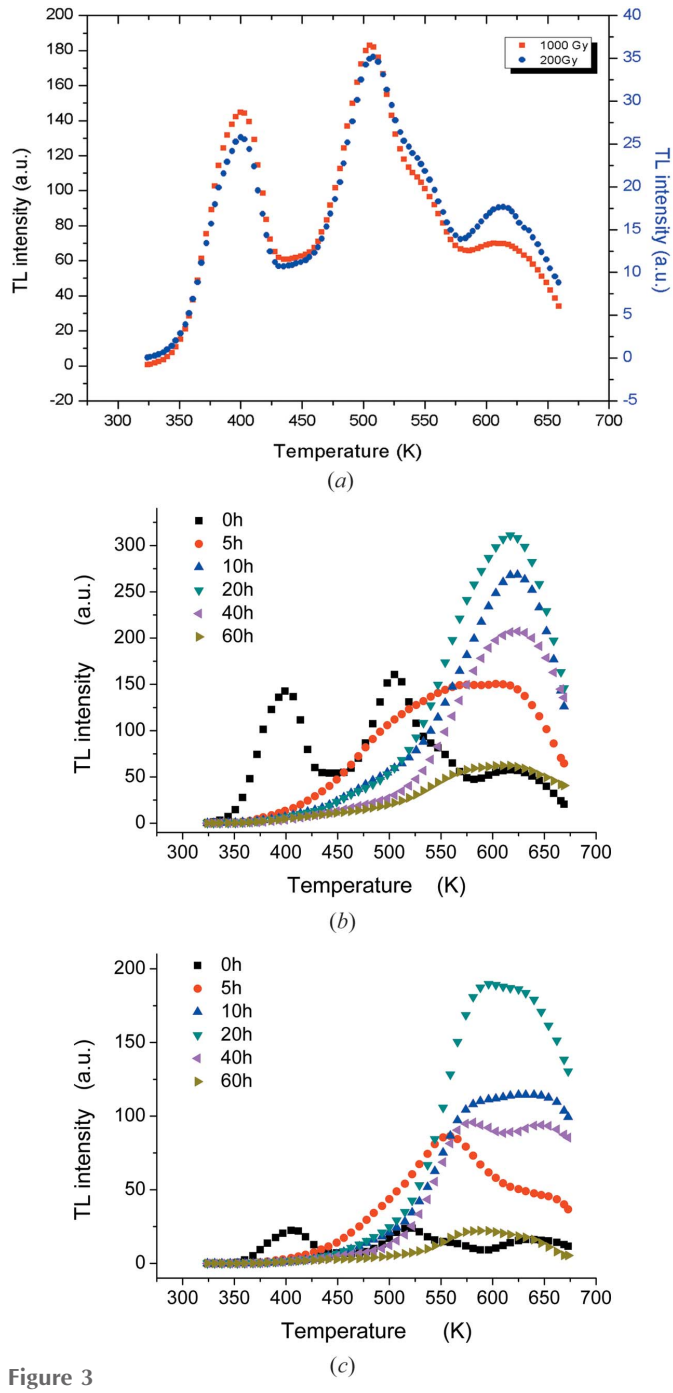

Figure 3
(*a*) Thermoluminescence glow curves for pristine LiF samples exposed to 200 Gy (circles, right axis) and 1000 Gy (squares, left axis) of γ-radiation. (*b*) Thermoluminescence glow curves for LiF samples exposed to 1000 Gy of γ-radiation. (*c*) Thermoluminescence glow curves for LiF samples exposed to 200 Gy of γ-radiation.

Table 1
Fitting parameters of six glow peaks resulting from the glow curve deconvolution using the 'first-order' kinetic model [equation (2)] of LiF samples irradiated at 200 Gy and 1000 Gy.

	LiF (1000 Gy)			LiF (200 Gy)		
Peak No.	Maximum intensity I_m (a.u)	Activation energy E (eV)	Temperature position T_m (K)	Maximum intensity I_m (a.u)	Activation energy E (eV)	Temperature position T_m (K)
1	36.01 ± 2	1.06 ± 0.05	380.03 ± 1	4.99 ± 0.3	1.11 ± 0.07	378.33 ± 0.59
2	114.9 ± 3.6	0.87 ± 0.01	400.83 ± 0.76	20.91 ± 1.51	0.84 ± 0.01	400.17 ± 0.76
3	48.4 ± 1.5	0.57 ± 0.01	432.50 ± 0.5	8.71 ± 0.34	0.57 ± 0.01	433 ± 1
4	116.87 ± 2	1.04 ± 0.04	500.50 ± 0.5	24.58 ± 1.01	1.04 ± 0.07	501.23 ± 0.64
5	83.32 ± 3	0.83 ± 0.06	532.40 ± 0.53	17.27 ± 0.86	1.03 ± 0.06	534.67 ± 0.58
6	70.47 ± 3.5	0.69 ± 0.01	610.70 ± 0.3	17.48 ± 0.93	0.72 ± 0.01	612 ± 1
FOM	0.96 ± 0.09			1.098 ± 0.15		

in K, E is the activation energy in eV, K is the Boltzmann constant in eV K^{-1}, $\Delta = 2KT(E)^{-1}$ and $\Delta_m = 2KT_m(E)^{-1}$.

Equation (2) has been used for curve fitting in the *Matlab* program to perform a non-linear least-squares fitting (Levenberg–Marquardt algorithm for minimization) in order to obtain the best refined values for E, T_m and I_m for each peak. The 'goodness of fitting' is judged by means of the figure of merit (FOM) index (Balian & Eddy, 1977), which is commonly used in all GCD algorithms for TL analysis (Bos *et al.*, 1994). The FOM index is defined as

$$\mathrm{FOM}\,[\%] = \frac{\sum_i^j |y_i - y(x_i)|}{A} \times 100, \qquad (3)$$

where i and j are the initial and ending temperatures in the fit region, respectively; y_i is the TL intensity at temperature position i, $y(x_i)$ is the value of the fit function at i, and A is the area under the peak, *i.e.* the integral of the fit function between i and j. It has been suggested that the fitting process is accurate if FOM has a value of 2.5% or less (Balian & Eddy, 1977).

The resultant GCDs of the pristine LiF sample irradiated at 200 Gy and 1000 Gy are shown in Fig. 4. As shown, the glow curves of both pristine LiF samples were easily deconvoluted into six glow peaks. Table 1 summarizes the resultant fitting parameters for all peaks along with the FOM of each fitting process for each sample. The FOM index results indicate a good and reliable fitting process.

Bearing in mind the mathematical uncertainty due to the deconvolution process, the peak position change due to uncontrolled non-ideal thermal contact of the sample's pellet with the heating element, and finally the temperature tolerance of the TLD reader (±1°), then the GCD results of both pristine LiF samples confirm their consistency with the 'first-order' kinetic model. The current result is consistent with the many results in the literature; for example, those obtained by Sagastibelza & Rivas (1981) who reported a spectrum of 15 'first-order' kinetic glow peaks of pure LiF for doses ranging from 2 to about 10^7 Gy. Baldacchini *et al.* (2008*a*) have studied pure crystals of LiF treated at different temperature and annealing conditions and up to ten 'first-order' kinetic peaks have been reported (Baldacchini *et al.*, 2008*b*). The dissimilarity in the number of peaks of the LiF glow curves in our case with that found in the literature originates from the discrepancy of the sample's origin and hence the inherent defect type.

On the other hand, the glow curves for all ball-milled samples acquire a broad TL spectrum at higher temperature which refers to continuum energy traps. Consequently, there are unlimited numbers of curve-fitting parameters that can yield the same glow curve. The phenomenon of continuum energy traps is usually associated with amorphous and highly defected samples (Chen & McKeever, 1997), hence the number of actual peaks of ball-milled samples cannot be inferred from curve fitting. Furthermore, each glow curve at dose 200 Gy differs significantly from its corresponding one at 1000 Gy in terms of peaks' positions and shapes [Figs. 3(*a*) and 3(*b*)]. Such significant discrepancies in

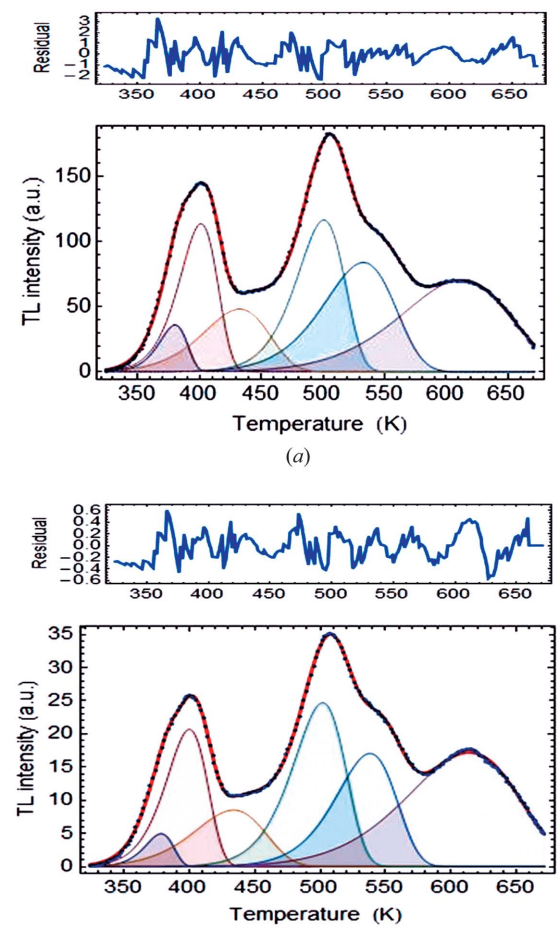

Figure 4
(*a*) Glow curve deconvolution of pristine LiF sample exposed to 1000 Gy using the 'first-order' kinetic model. Dots represent the experimental glow curve, individual peaks represent glow peaks deconvoluted by best fit and the solid line represents the superposition of deconvoluted glow peaks. FOM = 0.96 ± 0.09. (*b*) Glow curve deconvolution of pristine LiF samples exposed to 200 Gy using 'first-order' kinetic model. Dots represent the experimental glow curve, individual peaks represent glow peaks deconvoluted by best fit and the solid line represents the superposition of deconvoluted glow peaks. FOM = 1.098 ± 0.15.

the glow curves of all ball-milled samples, with respect to the pristine sample and with respect to each other, indicate that the inner mechanism of the TL process is departed from 'first-order' kinetics to other complicated kinetic models that cannot be easily inferred directly, neither from the TL glow curve nor from its curve fitting.

A general conclusion can be drawn here. The overall influence of the milling process on the TL phenomenon in terms of the traps density, as a direct parameter that affects the glow curve integral intensity, could be shortened to a few main points. First, a strong enhancement of the high-temperature traps and destruction for the low-temperature traps. Second, the enhancement of the high-temperature traps shows a dependency on the milling time. Lastly, milling induces a significant change in the microstructure that made the TL mechanism of a pure milled LiF unknown and unpredictable.

At this point, no more valuable information could be obtained from the TL glow curves; details about how the TL process takes place cannot be expected. Accordingly, additional results from an auxiliary technique that can explore the crystal defects (*e.g. in situ* XRPD) are needed to understand the mechanism of the TL process of highly defected ball-milled LiF samples.

3.2. XRPD analysis

For all pulverized LiF, a one-phase (fraction) WPPM model was sufficient and stable to fit the collected diffraction patterns, which relates to the samples' homogeneity. Starting from the pristine LiF powder, large crystallite sizes of about 500 nm coupled with an absence of dislocations were observed. After 5 h of milling, a strong decrease in the crystal size down to 36 (8) nm was observed, and the dislocation density was found to be about 4.4 (2) $\times$ 10^{15} m^{-2}. As the milling time increased, the crystal size did not show a strong difference in terms of average crystal size from 5 up to 60 h.

According to WPPM theory (Scardi & Leoni, 2002, 2004), the Wilkens factor (Wilkens, 1970) M [$M = \mathrm{Re}(\rho^{1/2})$] refers to the interactions among dislocations, where smaller M means a larger interaction is likely to take place at the crystal boundaries, and *vice versa*. The M values after 5, 10 and 20 h of milling were slightly above 1, then decreased after 40 and 60 h of milling to 0.89 and 0.77, respectively. The decrease of M with increasing milling time reveals that an extensive amount of lattice defects were introduced inside the crystals by increasing the milling duration. Fig. 5 shows the WPPM fitting of the LiF20h diffraction pattern as a witness of fitting quality, and Table 2 summarizes the most significant results of the WPPM modelling for all samples.

Table 2
Main WPPM results of LiF ball-milled at different milling times; estimated standard deviations are reported in parentheses and refer to the least significant digit.

Milling time (h)	Dislocation density 10^{15} m^{-2}	Crystallite size $\langle D \rangle$ (nm)	B contrast factor	Re (nm)	Wilkens factor [$M = \mathrm{Re}(\rho)^{1/2}$]
0		500			
5	4.4 (1)	36 (8)	−0.282 (4)	16 (1)	1.06 (1)
10	4.5 (2)	36 (5)	−0.284 (4)	16 (1)	1.07 (1)
20	4.8 (2)	36 (4)	−0.289 (5)	15 (1)	1.04 (1)
40	4.7 (2)	35 (5)	−0.284 (4)	13 (1)	0.89 (1)
60	7.3 (5)	34 (5)	−0.271 (8)	9 (1)	0.77 (2)

According to the TL results, the sample LiF20h showed the most intense TL response, which means that the density and type of defects responsible for the TL process are maximum. Accordingly, such a sample has been chosen for XRPD analysis to correlate the XRPD results with those of TL. *In situ* XRPD measurements were collected under non-isothermal conditions for LiF20h, starting from room temperature up to 900 K. Fig. 6 shows the *in situ* microstructure details of sample LiF20h collected by the imaging plate with a heating gradient of 10 K min^{-1}. The crystal growth at low temperature is little affected; the crystalline size, starting from roughly 35 nm, reaches approximately 100 nm at about 820 K. Around that temperature an enormous increase in the crystal size with a fast growth rate compared with the growth rate before 820 K

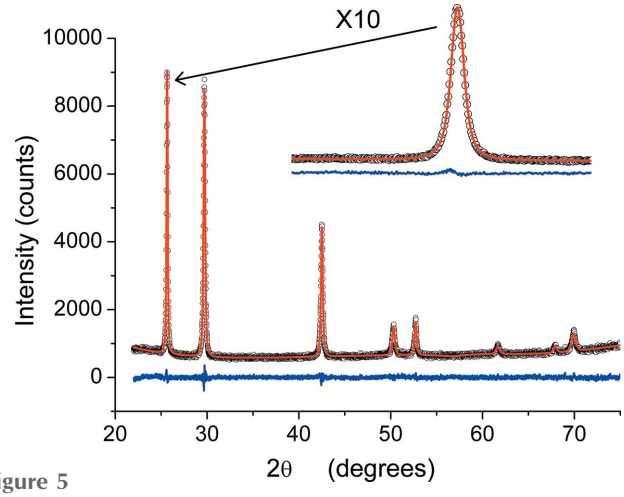

Figure 5
WPPM fitting for the LiF20h sample. The inset shows the fitting quality of the (111) crystalline plane zoomed in ten times. The open circles refer to the raw data; the continuous line refers to the fitting model and the line below refers to the residual.

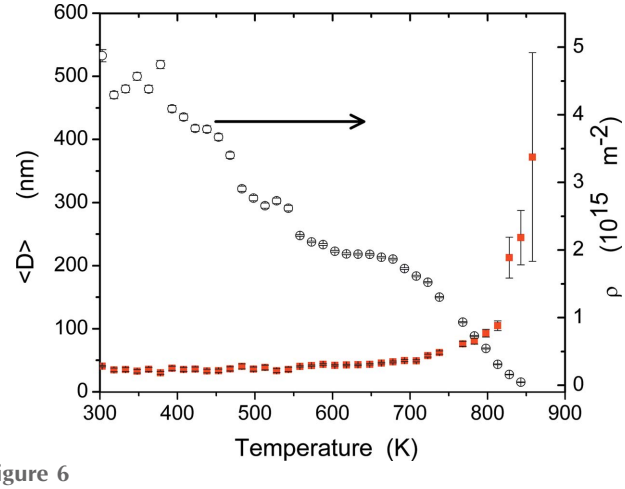

Figure 6
Changes in average crystallite size (solid squares) and dislocation density (open circles) for the LiF20h sample during non-isothermal *in situ* X-ray diffraction at a 10 K min^{-1} heating rate.

is found. The dislocation density is nearly constant up to ~425 K, which can be considered as a stability range for the pulverized LiF20h in which the dislocations probably arrange themselves to resist the temperature energy. Then, a recovery process takes place with a steady decrease in ρ until the temperature is high enough to start a recrystallization process (>820 K). A similar non-isothermal trend was observed in nanocrystalline ball-milled metallic and fluorite nanocrystalline compositions (Molinari *et al.*, 2010; Abdellatief *et al.*, 2014).

Fig. 7 reveals a correlation between the TL glow curve and the dislocation density as a function of temperature, even though it has to be mentioned that the heating rate is different in each experiment. The aforementioned disappearance of the low-temperatures traps after milling is actually located within the stability stage of dislocations (from room temperature to 425 K). Therefore, in the stability stage the electrons/holes traps seem to be constrained and interact with dislocations so they are less supporting to the TL process and consequently the first three peaks of the glow curve disappeared or relatively vanished. Then, a very broad peak started in coincidence with the beginning of the dislocations recovery process. This observation also supports the presence of the interaction between the electrons/holes and dislocations; while the dislocations density decreases as in the recovery stage, this interaction decreases which gives an increase to the appearance of the high-temperature traps. The intensity increase of the high-temperature traps for all pulverized LiF samples suggests that the grinding itself creates additional structural defects that increase the electrons/holes transitions density. These types of structural defect could enhance the TL response and most probably are point defects, but unfortunately XRPD does not provide quantitative information and/or confirmation to that; one way would be to test for the presence of point defects in the pulverized samples and to check the mechanism of dislocations recovery to determine whether or not point defects have a role in the dislocations recovery.

The dislocations recovery mechanism was studied at a selected point in the recovery region (*e.g.* 775 K) using the

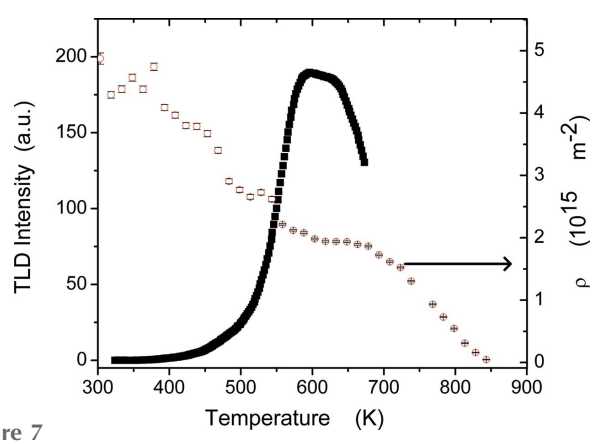

Figure 7
Correlation between the change in the dislocation density (open circles) and the thermoluminescence response (solid squares) of the LiF20h sample.

isothermal mode based on two different approaches (Liu & Evans, 1997) by tracking the rate of change of dislocation density. In the literature, there are several equations and methods that could be used to describe the recovery mechanism (Liu & Evans, 1997). The possible recovery mechanisms are diffusion-controlled dislocation glide, dislocation cross-slip, dislocation climb controlled by vacancy bulk diffusion or controlled by vacancy core diffusion. In one approach, ρ_t, the dislocation density at time t, divided by the initial dislocation density ρ_0 obeys equation (4) where the value of ρ_t was obtained from the WPPM analysis,

$$(\rho_t/\rho_0)^{1/2} = [1 + t/\tau]^{-m}. \quad (4)$$

Here, τ is the relaxation time parameter. The recovery mechanism type is determined according to the value of the parameter m retrieved from curve fitting of equation (4). The parameter m equals 1 when the mechanism is glide recovery with lateral jog drift; and m equals 0.5 or 0.25 when the mechanism is climb controlled by vacancy bulk diffusion or core diffusion, respectively. The last possible mechanism is cross slip at which m equals −1 (Liu & Evans, 1997).

Another approach that was used to obtain m is described by equation (5),

$$\alpha(t) = \frac{\rho_0 - \rho_t}{\rho_0 - \rho_f} = 1 - \exp\{-[k(T)t]^m\}. \quad (5)$$

In this equation, $\alpha(t)$ is the relative dislocation change at time t obtained from WPPM analysis of the isothermal treatment, ρ_f is the dislocations density at time infinity of the recovery process and was approximated to a complete dislocation relief as calculated from non-isothermal analysis (1×10^{14} m^{-2}), and $k(T)$ is the rate constant.

Figs. 8(*a*) and 8(*b*) show the results of the isothermal WPPM modelling of equations (4) and (5), respectively. Accordingly, equation (4) gives m = 0.24 (0.07) and relaxation parameter τ = 84 (37); this result declares that the dislocation recovery mechanism is climb controlled by vacancy core diffusion. Alternatively, equation (5) gives m = 0.55 (0.04); this value reveals that the recovery mechanism is climb controlled by vacancy bulk diffusion. The two approaches of tracing the dislocations recovery then confirm the presence of point defects and their interaction with dislocations. *In situ* X-ray diffraction measurement under isothermal conditions shows only about 50% of transformation and it must be highlighted that a complete kinetics study requires complete transformation which in turn needs much more experimental time. Therefore, the kinetics results within the current transformation range were obtained just to shed light on the most probable mechanism for dislocation recovery.

From the previous analysis, vacancies, which are responsible for hosting electrons and/or holes acting as traps centres, seem to be created by grinding together with dislocations. Very likely there is a certain interaction between vacancies and dislocations and that interaction makes them somehow bound to dislocations and do not participate in the TL response. This interaction decreases as dislocations decrease and thus explains why high-temperature traps are shown.

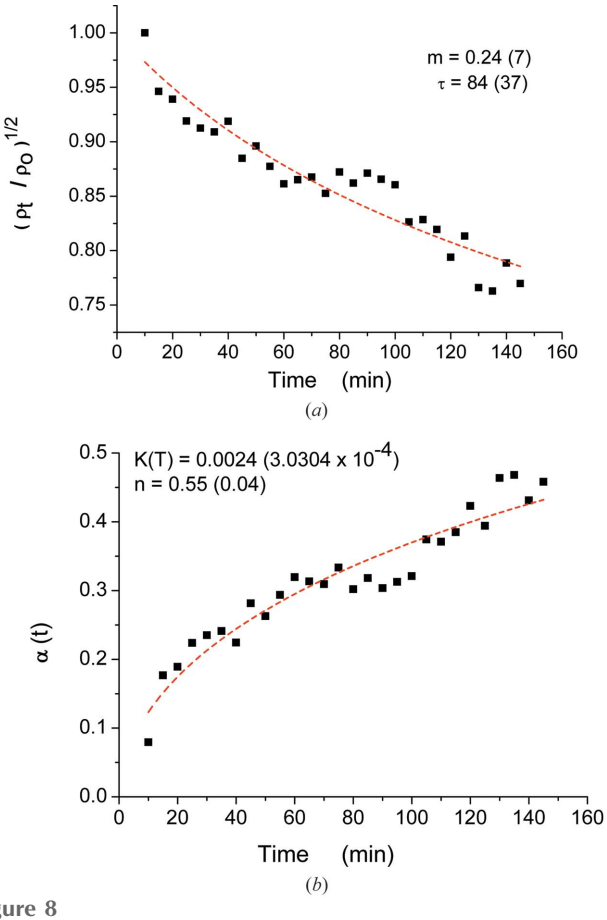

Figure 8
(*a*) Dislocation recovery in an isothermal treatment at 775 K [equation (4) approach]. (*b*) Dislocation recovery in an isothermal treatment at 775 K [equation (5) approach].

It is quite clear that the behaviour of the integral intensity shown in Fig. 2 for all-milled samples is mainly dominated by the behaviour of the fifth and sixth glow peaks at high temperature in the range 535–610 K, and all other peaks show a minor effect on the whole glow curve. For samples LiF5h, LiF10h and LiF20h, the overall density of the traps levels increased linearly. There is a possibility that, by increasing the milling time, the density of point defects that are responsible for the electrons/holes trapping process increases. Decreasing the integrated intensity after 20 h of milling (*i.e.* LiF40h and LiF60h) could be attributed to the increase in the interactions among the dislocations themselves whereas the Wilkens factor M decreased after 20 h of milling giving an indication of increasing the interactions among dislocations (Wilkens, 1970). The samples LiF40h and LiF60h have M values of less than unity, *i.e.* 0.89 and 0.77, respectively, unlike the other pulverized samples which have values larger than unity (see Table 2). So, increasing the dislocations–dislocations interaction possibly also increases the vacancies–dislocations interaction which in turn means binding more vacancies to dislocations and less vacancy density contributes to the TL mechanism. In any case, a further deep study on the TL ball-milling time dependence is required for a better understanding.

4. Conclusion

The influence of the microstructure of pulverized LiF on its TL response has been studied. The glow curve of the pristine LiF shows a minimum of six traps for electrons/holes. After milling, the LiF microstructure has been entirely changed in terms of crystal size and dislocations density. The crystal size decreased from >500 nm to about 34 nm and the dislocations density increased with milling to 7.3×10^{15} m^{-2} after 60 h of milling. Studying the dislocations recovery mechanism reveals that ball-milling has introduced point defects and dislocations to the ground samples. These point defects are playing a major role in the dislocations recovery process.

The grinding enhances the TL response at the high-temperature traps and weakens the low-temperature traps. The damping of the low-temperature traps was attributed to the presence of vacancies–dislocations interactions which decreases the number of vacancies that play a role in the TL response. This vacancies–dislocations interaction was strong at the stability stage of dislocations (from room temperature to 425 K) in which the dislocations show a stability with temperature. In the recovery stage (temperature >425 K), dislocations were decreasing and so the vacancies–dislocations interactions were consequently decreasing, which gave rise to the appearance of the high-temperature traps peaks.

The density of the traps was increasing with grinding, reaching a maximum value after 20 h of milling before starting to decrease for the LiF40h and LiF60h samples. The increasing of the overall traps density was attributed to the creation of more structural point defects with increasing milling times, which seems logical. On the other hand, decreasing the traps intensity after 20 h of milling could be related to increasing dislocations–dislocations interactions as deduced from decreasing the Wilkens factor for LiF40h and LiF60h as obtained from XRPD line profile analysis.

Acknowledgements

The authors would like to acknowledge both the International Centre for Theoretical Physics (ICTP) and the Elettra synchrotron facility for offering access to the synchrotron radiation facility Elettra-Sincrotrone through the ICTP-Elettra Users Programme for carrying out the synchrotron *in situ* XRPD experiments at the MCX beamline.

References

Abdellatief, M. (2013). PhD thesis, University of Trento, Italy (http://eprints-phd.biblio.unitn.it/979/).
Abdellatief, M., Lausi, A., Plaisier, J. R. & Scardi, P. (2014). *Metall. Mater. Trans. A*, **45**, 123–128.
Baldacchini, G., Chiacchiaretta, P., Gupta, V., Kalinov, V. & Voitovich, A. P. (2008*a*). *Phys. Solid State*, **50**, 1747–1755.
Baldacchini, G., Montereali, R. M., Nichelatti, E., Kalinov, V. S., Voitovich, A. P., Davidson, A. T. & Kozakiewicz, A. G. (2008*b*). *J. Appl. Phys.* **104**, 063712.
Balian, H. G. & Eddy, N. W. (1977). *Nucl. Instrum. Methods*, **145**, 389–395.
Bos, A. J. J., Piters, T. M., Gomez Ros, J. M. & Delgado, A. (1994). *Radiat. Prot. Dosim.* **51**, 257–264.

Chen, R. & McKeever, S. W. S. (1997). *Theory of Thermoluminescence and Related Phenomena*, Ch. 1 and 2. Singapore: World Scientific.
Garlick, G. F. J. & Gibson, A. F. (1948). *Proc. Phys. Soc.* **60**, 574–590.
Kirsh, Y. (1992). *Phys. Status Solidi A*, **129**, 15–48.
Kitis, G., Gomez-Ros, J. M. & Tuyn, J. W. N. (1998). *J. Phys. D*, **31**, 2636–2641.
Leoni, M., Confente, T. & Scardi, P. (2006). *Z. Kristallogr. Suppl.* **2006**, 249–254.
Liu, M. & Evans, B. (1997). *J. Geophys. Res.* **102**, 24801–24809.
May, C. E. & Partridge, J. A. (1964). *J. Chem. Phys.* **40**, 1401.
McKeever, S. W. S. (1983). *Thermoluminescence of Solids.* Cambridge University Press.
Molinari, A., Libardi, S., Leoni, M. & Scardi, P. (2010). *Acta Mater.* **58**, 963–966.
Randall, J. T. & Wilkins, M. H. F. (1945). *Proc. R. Soc. London A*, **184**, 366.
Rebuffi, L., Plaisier, J. R., Abdellatief, M., Lausi, A. & Scardi, P. (2014). *Z. Anorg. Allg. Chem.* **640**, 3100–3106.
Riello, P., Lausi, A., Macleod, J., Plaisier, J. R., Zerauschek, G. & Fornasiero, P. (2013). *J. Synchrotron Rad.* **20**, 194–196.
Sagastibelza, F. & Rivas, J. L. A. (1981). *J. Phys. C*, **14**, 1873–1889.
Scardi, P. & Leoni, M. (2002). *Acta Cryst.* A**58**, 190–200.
Scardi, P. & Leoni, M. (2004). *Whole Powder Pattern Modeling: Theory and Applications.* Berlin: Springer Verlag.
Sunta, C. M. (2015). *Unraveling Thermoluminescence, Springer Series in Materials Science*, Vol. 202. New York: Springer-Verlag.
Ungár, T., Dragomir, I., Révész, Á. & Borbély, A. (1999). *J. Appl. Cryst.* **32**, 992–1002.
Wall, C., Pohl, A., Knapp, M., Hahn, H. & Fichtner, M. (2014). *Powder Technol.* **264**, 409–417.
Wilkens, M. (1970). *Fundamental Aspects of Dislocation Theory*, edited by J. A. Simmons, R. de Wit and R. Bullough, Vol. II, pp. 1195–1221. National Bureau of Standards (US) Special Publication No. 317. Washington: National Bureau of Standards.